Sigma-Aldrich®
Lab & Production Materials

Application Note

Characterization and Performance Insights of Advanced Li-ion Cathode Materials

Exploring Layered NMC and LFP Cathode Materials

Manasi Mwemezi[1], Amir Chamaani[2]

[1]R&D and Customer Support Lab APAC (Daejeon, South Korea)

[2]Energy Storage and Battery Materials, Materials Science R&D (Milwaukee, WI, USA)

Abstract

This white paper presents materials characterization and electrochemical performance data for key lithium-ion cathode materials, including high- to moderate-nickel content layered oxide materials known as NMCs (NMC811, Al-doped NMC, and NMC532) and olivine-type Lithium Iron Phosphate (LFP). Structural and compositional analyses spanning particle morphology, phase purity, and elemental composition, along with physical parameters such as particle size distribution, surface area, and tap density, provide a detailed understanding of each material's attributes. Electrochemical evaluations further demonstrate clear differences in capacity, rate capability, and cycle stability, underscoring the strengths and trade-offs of various cathode compositions with distinct performance profiles. Together, these findings provide a data-driven foundation for selecting cathode materials optimized for specific performance needs.

Introduction

Lithium-ion batteries (LIBs) have become the dominant rechargeable energy storage technology, powering devices from smartphones to electric vehicles (EVs). Their widespread adoption is driven by high energy density, long cycle life, and decreasing production costs. As the transition toward electrification accelerates, there is increasing pressure on manufacturers and researchers to enhance battery performance, safety, and sustainability.

A critical component influencing a battery's energy density, voltage output, safety, and cost is the cathode active material (CAM). Among commercially relevant CAM chemistries, nickel-rich layered oxides, such as nickel-manganese-cobalt (NMC) variants like NMC811 and NMC532, have gained prominence for high specific capacity and extended driving range in EVs. NMC811, with its high nickel content, offers greater capacity and energy density but poses challenges in thermal stability and cycle life. In contrast, NMC532 provides a more balanced composition, delivering slightly lower energy density but improved structural stability and safety.

To address the weaknesses of nickel-rich cathodes, doping strategies such as aluminum doping in NMC811 have been introduced. This approach enhances structural integrity and reduces undesirable phase transitions, leading to improved cycle life and high-temperature performance while retaining significant capacity advantages.

Additionally, lithium iron phosphate ($LiFePO_4$, LFP) serves a distinct market segment. Although it has lower energy density compared to NMC chemistries, LFP is recognized for its exceptional thermal stability, long service life, and lower raw material costs, making it suitable for applications prioritizing safety and durability over maximum range.

This paper presents a comprehensive analysis of essential lithium-ion cathode materials, focusing on high- to moderate-nickel content layered oxides, including NMC811, aluminum-doped NMC, and NMC532, alongside LFP. Structural and compositional analyses, including particle morphology, phase purity, and elemental composition, are complemented by physical parameters such as particle size distribution and tap density. Electrochemical evaluations further reveal differences in capacity, rate capability, and cycle stability, providing a data-driven foundation for selecting cathode materials optimized for specific performance needs.

Experimental

Materials

Cathode active materials (NMCs and LFP), carbon Super C65, N-methyl-2-pyrrolidone (NMP) solvent, and electrolyte were internally sourced from Merck KGaA, Darmstadt, Germany. NMC electrodes were fabricated using a 90:5:5 weight ratio of active material, Super C65 carbon, and polyvinylidene fluoride binder (PVDF, Kynar® HSV900), while LFP electrodes followed a 94:3:3 formulation. NMC and LFP electrodes were coated on aluminum foil (16 µm) and conductive carbon-coated aluminum foil (18 µm) respectively, calendared to a porosity of 30–40%, with mass loadings corresponding to areal capacities of 1–2 mAh/cm². The electrolyte consisted of 1 m $LiPF_6$ in a 1:1:1 volumetric mixture of ethylene carbonate (EC), diethyl carbonate (DEC), and dimethyl carbonate (DMC), and Celgard® 2325 (tri-layered PP/PE/PP) was used as the separator.

Cathode Materials Characterization

The cathode materials were characterized to assess their physical, structural, and compositional properties. Surface morphology and particle shape were examined by scanning electron microscopy (SEM). Crystallographic structure was determined by powder X-ray diffraction (XRD), and elemental composition and impurities were quantified by inductively coupled plasma coupled to mass spectrometry (ICP-MS) analysis. Particle size distribution, specific surface area, and tap density were also measured to evaluate packing behavior and surface-related properties. Differential Scanning Calorimetry (DSC) was utilized to investigate the thermal properties of the electrode materials by measuring changes in heat flow as a function of time and temperature.

Electrochemical Characterization

Electrodes were prepared by casting a slurry containing the active material, conductive carbon, and PVDF binder in NMP onto aluminum foil. The coated electrodes were initially dried for 6 hours at 80 °C, followed by overnight vacuum drying at the same temperature. The electrodes were then calendered and punched into circular discs for coin cell assembly.

CR2032 coin cells were assembled in an argon-filled glovebox using lithium metal as both the counter and reference electrode. After assembly, the cells were rested for 24 hours prior to electrochemical analysis. Formation was conducted using one initial charge/discharge cycle at C/20, followed by two cycles at C/10 for the NMC cathodes. For the LFP cathode, there were two charge/discharge cycles at C/10, followed by one cycle at C/5. All subsequent charge steps employed a constant current—constant voltage (CC–CV) protocol, with the CV step terminated at a cutoff current of C/20. All electrochemical analysis was carried out at room temperature.

Rate capability was evaluated by charging at C/3 and discharging at increasing rates from C/5 to 5C for NMC cathodes and from 1C to 5C for LFP cathode, with each rate maintained for five consecutive cycles. Long-term cycling stability was assessed at a constant charge and discharge rate of C/3.

Results and Discussion

Tables 1 and **2** summarize the chemical composition, impurity levels, surface area, tap density, and median particle size of three NMCs along with LFP cathode materials. ICP analysis shows that both NMC811 and Al-doped NMC (aka NMCA) have high nickel content, with compositional ratios of approximately Ni:Mn:Co of 8.5:0.5:1.0 and Ni:Mn:Co:Al of 9.0:0.4:0.6:0.1, respectively. This high nickel content is tailored to achieve high specific capacities, stemming from the nickel redox activity that enables greater lithium extraction per formula unit. The composition of NMC532 features a more balanced Ni:Co:Mn ratio, providing moderate capacity while ensuring greater stability. Cobalt contributes to electronic conductivity, while manganese ensures structural stability during cycling. On the other hand, LFP, composed mainly of iron and phosphate, demonstrates excellent purity, supporting its consistent electrochemical performance (vide infra). Trace Ti (387.6 ppm) was detected in LFP, originating from naturally occurring minerals in the precursor. Titanium is sometimes intentionally added to improve electrochemical performance, and the level observed here is well below typical doping amounts, posing no risk to performance or safety.[13,14] CHNS elemental analysis of the LFP also indicates the carbon is <1.5 wt.% and sulfur 0.4 wt.%. The low carbon level is consistent with a thin conductive carbon coating, while the low sulfur content suggests minimal sulfate or sulfur-bearing impurities.

Overall, all NMCs and LFP materials exhibit very low levels of impurities, confirming their high purity. Physical measurements such as particle size, surface area, and packing density indicate well-controlled morphology and size distributions, which support uniform electrode packing and predictable porosity, enabling efficient electrolyte wetting and Li-ion transport while limiting parasitic surface reactions. Consequently, the cathode material powders are suitable for stable and reproducible electrochemical behavior.

Table 1. Chemical Composition Analyzed by ICP and Physical Properties of NMC (ND: Not Detected; N/A: Not Available)

Description		Unit	Materials		
			NMC532	NMC811	NMCA
Chemistry	Ni	mol.%	5.5	8.4	8.9
	Mn	mol.%	2.6	0.4	0.4
	Co	mol.%	1.8	1.2	0.6
	Al	mol.%	N/A	N/A	0.07
Impurities	Fe	ppm	ND	ND	3.0
	Cr	ppm	1.8	1.6	6.0
	Na	ppm	37.6	12.4	7.1
	Cu	ppm	ND	ND	9.3
	Zn	ppm	ND	ND	ND
BET Surface area		m^2/g	0.36	0.49	0.6
Tap Density		g/cm^3	2.32	2.69	2.5
PSD	D50	µm	8.99	9.97	11.3

Table 2. Chemical Composition Analyzed by ICP and Physical Properties of LFP Cathode (ND:Not Detected ; N/A: Not Available)

Description		Unit	Materials
			LFP
Chemistry	Li	wt. %	4.29
	P	wt. %	19.57
	Fe	wt. %	34.29
	C	Wt. %	<1.5
	S	Wt. %	0.4
Impurities	Al	ppm	27.6
	Ca	ppm	19.3
	Co	ppm	ND
	Cr	ppm	ND
	Cu	ppm	ND
	Mg	ppm	3.6
	Mn	ppm	8.0
	Ni	ppm	ND
	Pb	ppm	ND
	Ti	ppm	387.6
	Zn	ppm	7.4
	Na	ppm	ND
	K	ppm	ND
BET Surface area		m2/g	14
Tap Density		g/cm^3	0.8
PSD	D50	µm	1.2

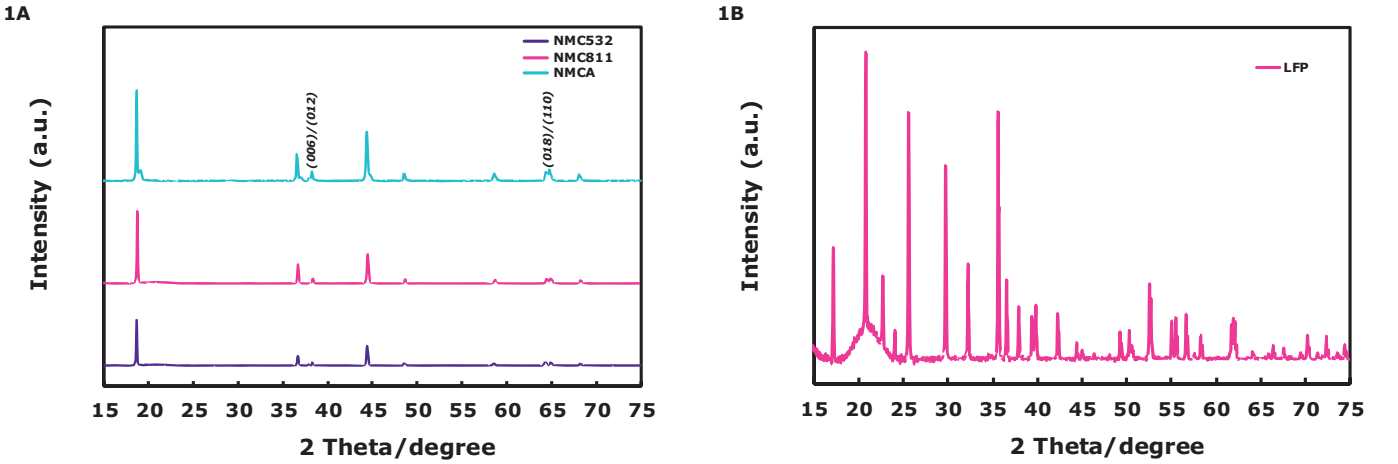

Figures 1A and 1B. X-ray diffraction (XRD) patterns of NMC-based materials NMC532, NMC811, and NMCA (1A) and LFP (1B), highlighting phase composition and crystallinity.

Figure 1 shows the XRD patterns of all NMCs and LFP cathode materials. For the NMC cathode materials (**Figure 1A**), all peaks are indexed to the rhombohedral system with R3-m space group, and no additional peaks are observed between 20–30 degrees, indicating the absence of major phase impurities. All NMCs also show sharp peaks with the distinct doublet-peak splits for the (006)/(102) and (108)/(110) observed around 37° and 64°, respectively. This indicates well-ordered crystalline structures of NMC materials. Notably, the NMCA's peaks were slightly more intense and narrower compared to NMC811, suggesting improved crystallinity due to Al incorporation (**Figure 1B**). All XRD peaks of LFP in **Figure 1B** are indexed to an ordered olivine structure with a Pnma space group. The diffraction pattern of LFP with carbon coating did not significantly affect the structure of $LiFePO_4$.

SEM images of the layered oxide materials revealed well-defined spherical secondary particles composed of aggregated primary crystallites (**Figure 2**). NMC532 exhibited densely packed primary particles, while NMC811 showed a slightly looser arrangement (Figures 2A and 2B). Such morphological differences are consistent with their typical electrochemical characteristics, where the more open structure of NMC811 facilitates faster lithium-ion transport and higher specific capacity due to its high nickel content, while the denser packing in NMC532 improves structural integrity during extended cycling.[15–17] Al-doped NCM (NMCA) also revealed larger secondary particles (**Figure 2C**) indicating that aluminum incorporation may influence particle growth.[9,10]

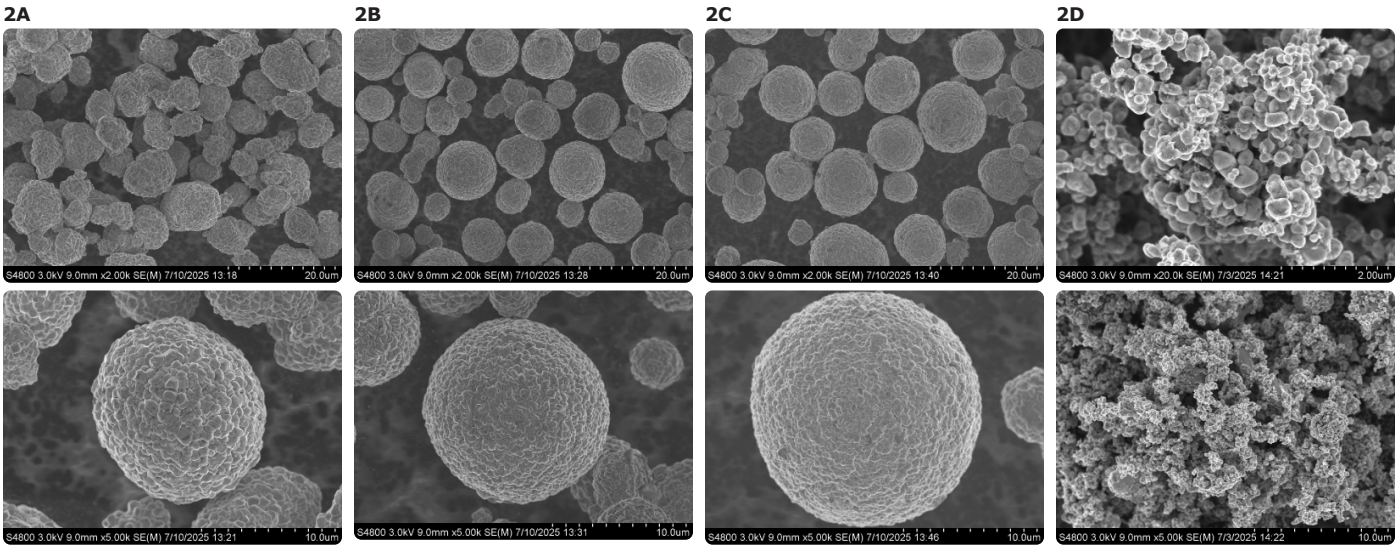

Figures 2A to **2D**. Scanning Electron Microscopy (SEM) images of cathode materials: NMC532 (**2A**), NMC811 (**2B**), Al-doped NMC811 (**2C**), and Lithium Iron Phosphate (LFP) (**2D**), showing morphology and structure at various magnifications.

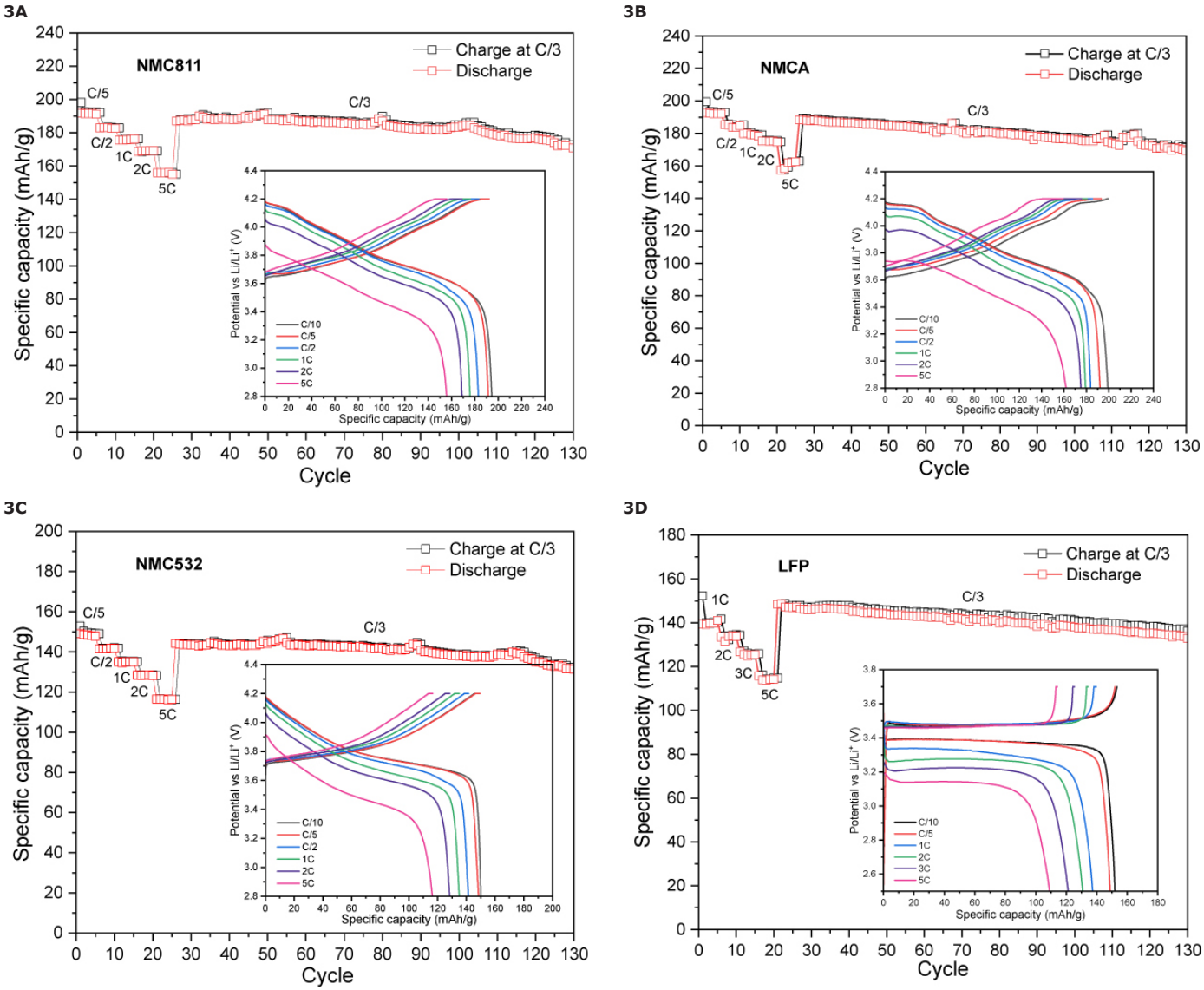

Figures 3A to 3D. Specific capacity vs. cycle number for NMC811 (**3A**), NMCA (**3B**), NMC532 (**3C**), and LFP (**3D**), showing discharge performance at different rates with a constant C/3 charge, as well as long-term cycling at C/3 charge-discharge.

In contrast, the SEM images of LFP (**Figure 2D**) reveal an aggregated network of irregularly shaped primary particles, forming porous secondary agglomerates. This morphology is characteristic of olivine-type LFP and supports stable cycling performance by enabling structural robustness and steady lithium-ion diffusion pathways, although it generally exhibits lower electronic conductivity compared to layered oxides.[11,18]

To assess the electrochemical performance and practical capacity of cathode materials, coin cells using lithium metal as both the counter and reference electrode were tested. The NMCs and LFP cells were tested in the voltage range of 2.8-4.2 V and 2.0-3.7 V vs Li/Li+, respectively. **Figure 3** displays their discharge capacities at different C-rates with a constant C/3 charge, along with their long-term cycling at C/3 charge/discharge. Across all measured C-rates, the high nickel content NMCs (NMC811 and NMCA) delivered higher absolute discharge capacities than the mid-range one (NMC532). NMC811 achieved 194 mAh/g at C/10, 191 mAh/g at C/5, 183 mAh/g at C/2, 176 mAh/g at 1C, 169 mAh/g at 2C, and 156 mAh/g at 5C (**Figure 3A**). NMCA delivered 199 mAh/g at C/10, 192 mAh/g at C/5, 184 mAh/g at C/2, 179 mAh/g at 1C, 175 mAh/g at 2C and 162 mAh/g at 5C (**Figure 3B**). The discharge capacities of NMC532 were 150 mAh/g at C/10, 148 mAh/g at C/5, 141 mAh/g at C/2, 135 mAh/g at 1C, 128 mAh/g at 2C, and 116 mAh/g at 5C (**Figure 3C**). The initial coulombic efficiencies of NMC811, NMC532 and NMCA were in the range of 85 to 90%.

During extended cycling, NMC811 maintained an absolute capacity of approximately 166 mAh/g after 100 cycles, while NMC532 retained about 126 mAh/g under identical conditions. The higher discharge capacities of NMC811 in both rate and cycling tests are consistent with its higher nickel content and greater lithium-ion diffusivity, although interpretation of long-term stability trends under these specific test parameters for all NMCs is beyond the scope of the current work.

LFP exhibited a first-cycle capacity of 153 mAh/g at C/10 with a notably higher Initial Coulombic Efficiency (ICE) of 97.5% compared to both NMCs (**Figure 3D**). This is due to LFP's excellent electrochemical stability, lower reactivity, favorable phase transition behavior, and stable lithium-ion diffusion pathways, which minimize capacity loss even during the first cycle.

At higher C-rates, LFP delivered 150 mAh/g at C/5, 140 mAh/g at 1C, 134 mAh/g at 2C, 125 mAh/g at 3C, and 114 mAh/g at 5C. Over extended cycles, LFP retained approximately 140 mAh/g after 100 cycles, with its stable capacity retention attributable to the robust olivine lattice and uniform particle network observed in the SEM analysis. These features mitigate structural degradation and capacity fading, enabling LFP to sustain more consistent performance over prolonged cycling compared to the layered NMC counterparts.

The electrochemical performance of NMC532, NMC811 and NMCA was further evaluated under different charge cut-off voltages to assess their capacity, rate capability, and cycling stability.

NMC811 at a cut-off voltage of 4.2 V exhibited excellent cycling stability, with almost no capacity fade observed

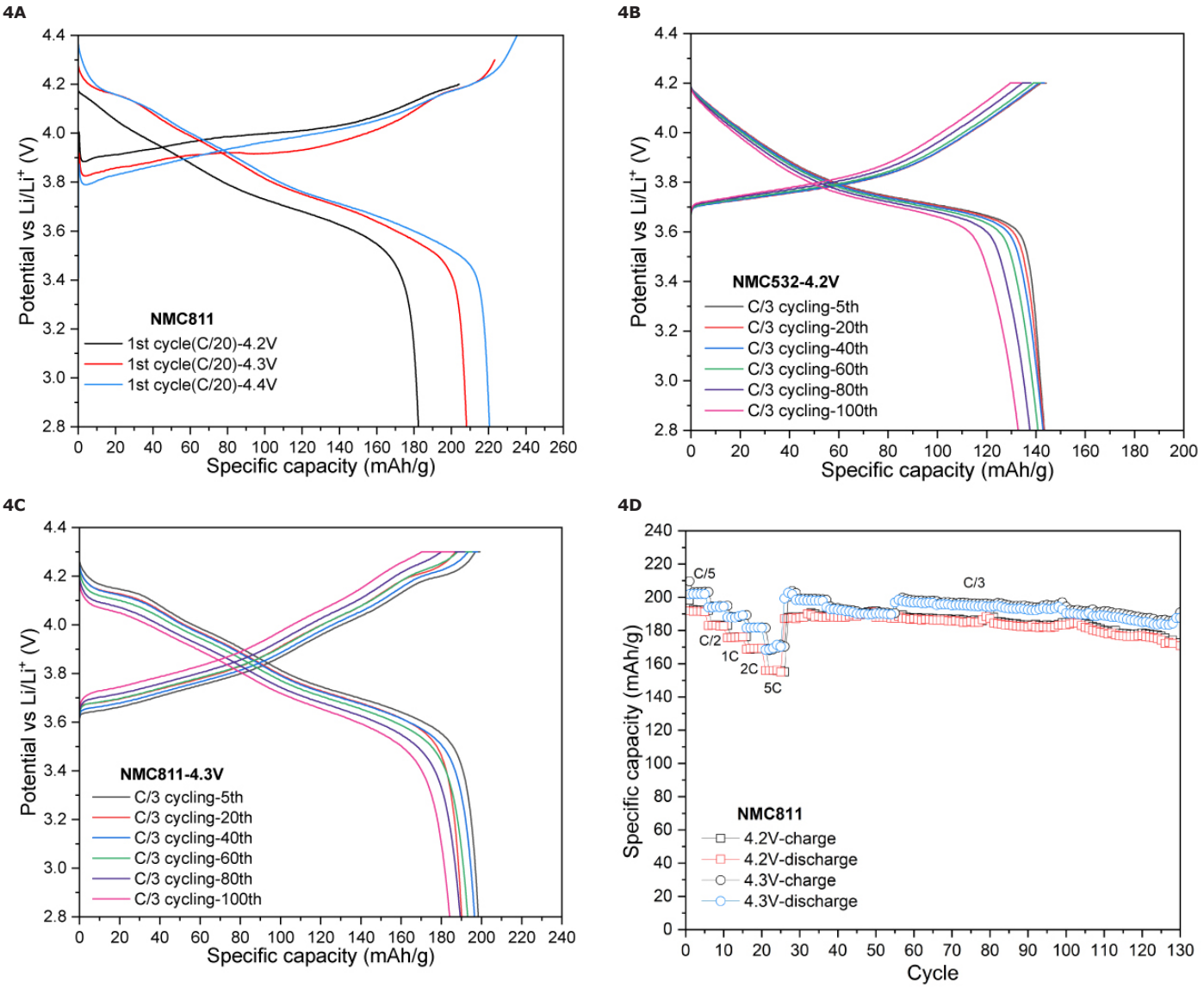

Figures 4A to 4D. Charge–discharge profiles of NMC811 at C/20 charge and discharge rate with upper voltage cutoffs of 4.2 V, 4.3 V, and 4.4 V (4A) Cycling performance at 4.2 V (4B) and 4.3 V (4C) cutoffs over 100 cycles at C/3 charge and discharge rate. (4D) Rate capability at various discharge C-rates with a constant C/3 charge rate along with long-term cycling at C/3 charge and discharge rate for 4.2 V and 4.3 V cutoffs.

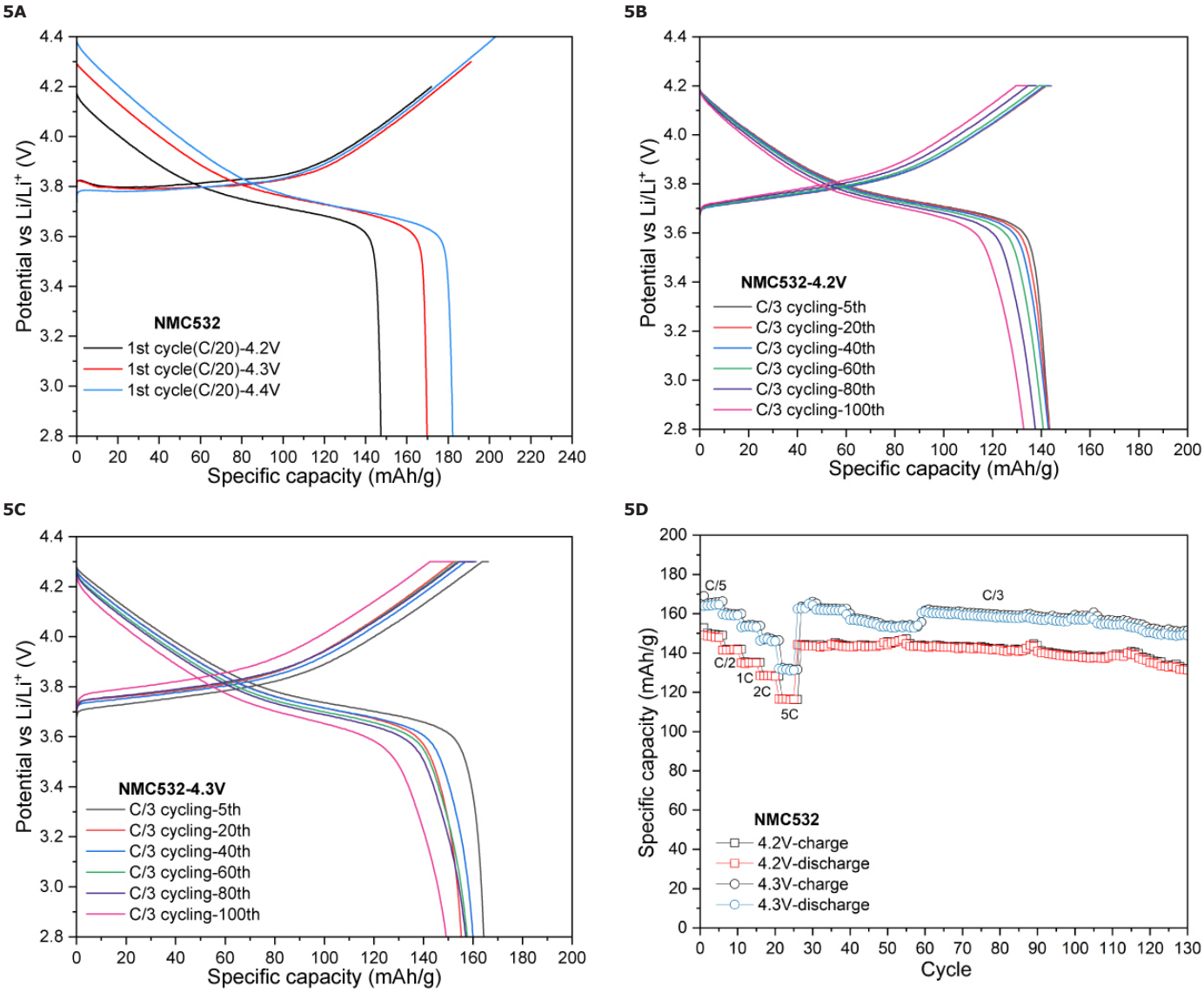

Figures 5A to **5D**. Charge–discharge profiles of NMC532 at C/20 with upper voltage cutoffs of 4.2 V, 4.3 V, and 4.4 V (5A), and at 4.2 V (5B) and 4.3 V (5C) cutoffs, demonstrating electrochemical performance over multiple cycles at C/3. (5D) Long-term cycling at C/3 for 4.2 V and 4.3 V cutoffs.

over 20 cycles. The electrode delivered a discharge capacity of 174 mAh/g, achieving a capacity retention of 93% after 100 cycles. When the cut-off voltage was increased to 4.3 V, the electrode retained a reversible capacity of 184 mAh/g after 100 cycles, corresponding to a capacity retention of 91.1%. Lastly, increasing the charge cut-off voltage to 4.4 V resulted in a significant boost in charge and discharge capacities, reaching 235 mAh/g and 220 mAh/g, respectively (**Figure 4**).

For NMC532, cycling at a 4.2 V cut-off resulted in a reversible capacity of 133 mAh/g after 100 cycles, corresponding to a capacity retention of 92.3%. At a slightly higher cut-off voltage of 4.3 V, the electrode retained 149 mAh/g, achieving a capacity retention of 91.0% after the same number of cycles. When the charge cut-off voltage was increased to 4.4 V, the charge and discharge capacities significantly improved, reaching 203/182 mAh/g, indicating enhanced performance at elevated voltage (**Figure 5**).

In **Figure 6**, NMCA was evaluated under similar conditions to assess the impact of Al-doping. Cycling at a cut-off voltage of 4.3 V, NMCA yielded a reversible capacity of 178 mAh/g after 100 cycles, resulting in a capacity retention of 89.5%. When tested at a slightly lower cut-off voltage of 4.2 V, the electrode demonstrated a capacity of 170 mAh/g, achieving

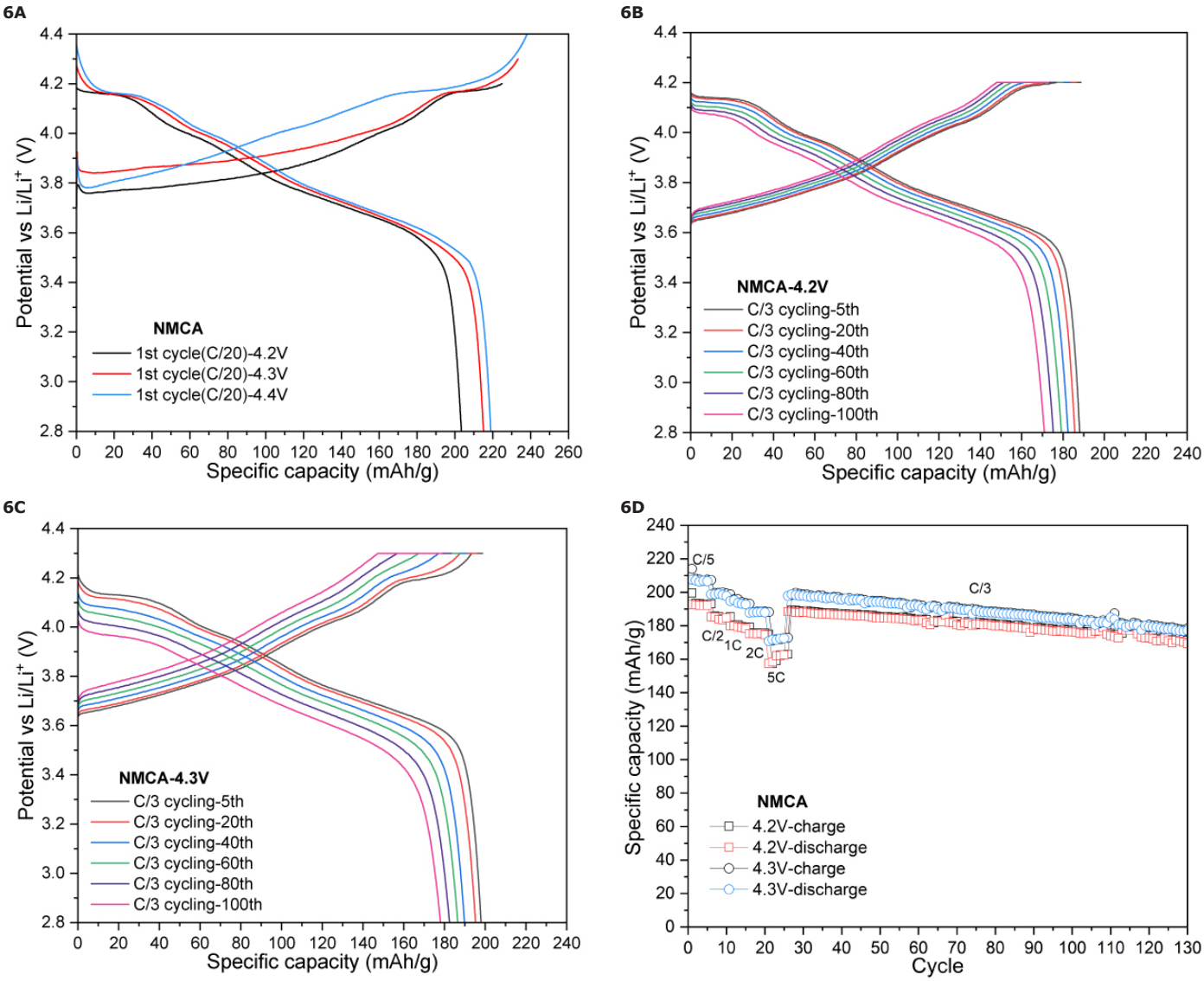

Figures 6A to 6D. Charge–discharge profiles of NMCA at C/20 charge and discharge rate with upper voltage cutoffs of 4.2 V, 4.3 V, and 4.4 V (6A). Cycling performance at 4.2 V (6B) and 4.3 V (6C) cutoffs over 100 cycles at C/3 charge and discharge rate. (6D) Rate capability at various discharge C-rates with a constant C/3 charge along with long-term cycling at C/3 charge and discharge rate for 4.2 V and 4.3 V cutoffs.

a retention of 90.2% after the same cycling period. Furthermore, increasing the cut-off voltage to 4.4 V resulted in significant enhancements in both charge and discharge capacities, reaching 238 mAh/g and 219 mAh/g, respectively.

Overall, these findings confirm that NMC-based cathode materials exhibit improved capacity and satisfactory cycling stability at higher cut-off voltages. However, there is a noticeable trade-off between increased capacity and capacity retention, which is more pronounced in the higher-nickel NMCs.

To evaluate the thermal stability of the NMCs and LFP cathode materials at elevated temperature, all samples were assembled into half coin cells and then were first subjected to one formation cycle at C/20 (charge/discharge), followed by charging to 4.2 V for NMCs and 3.7 V for LFP. Afterward, the cells were disassembled in an argon-filled glovebox, and the electrodes were thoroughly rinsed with dimethyl carbonate (DMC) and dried at room temperature. The cathode materials were then carefully scraped from the current collectors and sealed in hermetic pans for differential scanning calorimetry (DSC) measurements. The DSC experiments were conducted from 20 °C to 350 °C at a heating rate of 10 °C/min (**Figure 7**).

The DSC profiles of all NMCs and LFP display an endothermic peak around 180 °C, corresponding to the melting transition of the PVDF binder. The onset temperature, peak temperature, and shape of the

exothermic features provide insights into their relative thermal stability. In the case of layered NMC cathode materials, the exothermic behavior primarily results from the structural degradation of the delithiated cathode and subsequent oxygen release. As the temperature increases, the layered structure transitions to spinel- or rock-salt-like phases, destabilizing the lattice oxygen. The temperature and intensity of this peak are strongly influenced by the nickel content, with higher nickel concentrations leading to earlier and sharper exothermic peaks.[19–21] NMCA, which has the highest nickel content, exhibited the lowest onset temperature at approximately 197 °C, accompanied by a sharp and intense exothermic peak around 210 °C. In contrast, NMC811 and NMC532 displayed onset temperatures of 215 °C and 253 °C, respectively, with broad peaks occurring at approximately 238 °C and 284 °C. This suggests that the lower nickel content in the layered NMC cathode materials is associated with higher thermal stability. The sharper and narrower peak for NMCA indicates rapid and violent decomposition within a very limited temperature range, resulting in a much faster rate of heat release compared to NMC811 and NMC532. Additionally, the exothermic peak for NMC532 is broader than that of NMC811, suggesting a slower heat release during decomposition. All NMCs exothermic peaks exhibited shoulders reflecting the multi-step phase changes and oxygen release.[20–22]

LFP exhibited no significant exothermic activity until temperatures exceeded 240 °C, with any subsequent heat release being weak and very broad, indicating high thermal stability. This stability can be attributed to the strong P-O bonds within the olivine structure, which effectively suppress lattice oxygen release.[19,22]

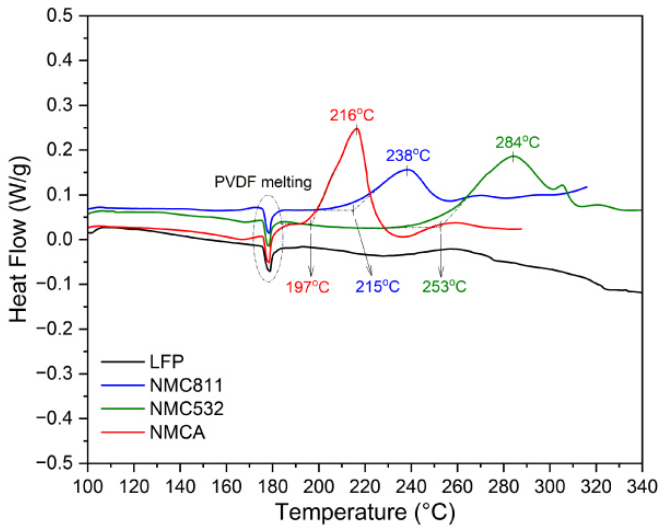

Figure 7. DSC curves for NMCs (NMC811, NMC532, and NMCA) and LFP, were obtained after charging at 4.2 V and 3.7 V versus Li/Li^+, respectively.

Conclusion

This study conducted extensive structural, compositional, and physical characterization of our recently commercialized Li-ion cathode materials—with a focus on high to mid nickel content layered oxides (NMC811, Al-doped NMC, and NMC532) and olivine-type LFP. This comprehensive analysis lays the groundwork for data-driven material selection. Electrochemical performance testing revealed that higher nickel content in NMCs (especially NMC811 and the Al-doped version) generally delivers higher discharge capacities at various C-rates compared to NMC532. However, these benefits come with trade-offs in thermal stability and long-term capacity retention. Among them, LFP, driven by its strong olivine structure and lower energy density, offers superior thermal stability, which is valuable for safety-critical applications.

References

1. Ngoy KR, Lukong VT, Yoro KO, Makambo JB, Chukwuati NC, Ibegbulam C, Eterigho-Ikelegbe O, Ukoba K, Jen TC. 2023. Lithium-ion batteries and the future of sustainable energy: a comprehensive review. Renew Sustain Energy Rev. 223:115971. **https://doi.org/10.1016/j.rser.2025.115971**
2. Parvizi P, Jalilian M, Mohammadi Amidi A, Zangeneh MR, Riba JR. 2025. From present innovations to future potential: the promising journey of lithium-ion batteries. Micromechanics. 16(2):194. **https://doi.org/10.3390/mi16020194**
3. Hasan MM, Haque R, Jahirul MI, Rasul MG, Fattah IMR, Hassan NMS, Mofijur M. 2025. Advancing energy storage: the future trajectory of lithium-ion battery technologies. Energy Storage. 5:116511. **https://doi.org/10.1016/j.est.2025.116511**
4. Goodenough JB, Park KS. 2013. The Li-ion rechargeable battery: a perspective. J Am Chem Soc. 135(4):1167–76. **https://doi.org/10.1021/ja3091438**
5. Nykvist B, Nilsson M. 2015. Rapidly falling costs of battery packs for electric vehicles. Nat Clim Chang. 5:329–32. **https://doi.org/10.1038/nclimate2564**
6. Peters JF, Baumann M, Zimmermann B, Braun J, Weil M. 2017. The environmental impact of Li-ion batteries and the role of key parameters – a review. Renew Sustain Energy Rev. 67:491 – 506. **https://doi.org/10.1016/j.rser.2016.08.039**
7. Wood DL, Li J, Daniel C. 2015. Prospects for reducing the processing cost of lithium ion batteries. J Power Sources. 275:234 – 42. **https://doi.org/10.1016/j.jpowsour.2014.11.019**
8. Li W, Erickson EM, Manthiram A. 2020. High-nickel layered oxide cathodes for lithium-based automotive batteries. Nat Energy. 5(1):26 – 34. **https://doi.org/10.1038/s41560-019-0513-0**
9. Zhou K, Xie Q, Li B, Manthiram A. 2021. An in-depth understanding of the effect of aluminum doping in high-nickel cathodes for lithium-ion batteries. Energy Storage Mater. 34:229 – 40. **https://doi.org/10.1016/j.ensm.2020.09.015**
10. Jeong M, Kim H, Lee W, Ahn SJ, Lee E, Yoon WS. 2020. Stabilizing effects of Al-doping on Ni-rich LiNi0.80Co0.15Mn0.05O2 cathode for Li rechargeable batteries. J Power Sources. 474:228592. **https://doi.org/10.1016/j.jpowsour.2020.228592**
11. Padhi AK, Nanjundaswamy KS, Goodenough JB. 1997. Phosphate-based cathode materials for lithium-ion batteries. J Electrochem Soc. 144(4):1188 – 94. **https://doi.org/10.1149/1.1837571**
12. Hu J, Huang W, Yang L, Pan F. 2020. Structure and performance of the $LiFePO_4$ cathode material: from the bulk to the surface. Nanoscale. 12:15036 – 44. **https://doi.org/10.1039/D0NR03776A**
13. Zhang F, Huang J, Zong F, Tuo K, Cai X, Zhou X, Zhao D, Cui X, Li S, Zhang N. 2023. Effect of Ti content on preparation of $LiFePO_4$ cathode from $FeSO_4{\cdot}7\ h_2O$ waste residue. J Alloys Compd. 955:170270. **https://doi.org/10.1016/j.jallcom.2023.170270**

14. Li P, Wang Y, Liu W, Chen T, Liu K. 2025. Enhancing the structural and electrochemical properties of lithium iron phosphate via titanium doping during precursor synthesis. Energies. 18(4):930. **https://doi.org/10.3390/en18040930**

15. Li J, Cameron AR, Li H, Glazier S, Xiong D, Chatzidakis M, Allen J, Botton GA, Dahn JR. 2017. Comparison of single crystal and polycrystalline LiNi0.5Mn0.3Co0.2O2 positive electrode materials for high voltage Li-ion cells. J Electrochem Soc. 164(7):A1534 – 44. **https://doi.org/10.1149/2.0991707jes**

16. Shishvan SS, Fleck NA, McMeeking RM, Deshpande VS. 2023. Cracking and associated volumetric expansion of NMC811 secondary particles. J Power Sources. 588:233745. **https://doi.org/10.1016/j.jpowsour.2023.233745**

17. Son SB, Robertson D, Tsai Y, Trask S, Dunlop A, Bloom I. 2020. Systematic study of the cathode compositional dependency of cross-talk behavior in Li-ion battery. J Electrochem Soc. 167:160508. **https://doi.org/10.1149/1945-7111/abcb40**

18. Lu Y, Zhu T. 2024. Status and prospects of lithium iron phosphate manufacturing in the lithium battery industry. MRS Commun. 14:888 – 99. **https://doi.org/10.1557/s43579-024-00644-2**

19. Samigullin RR, Drozhzhin OA, Antipov EV. 2022. Comparative study of the thermal stability of electrode materials for Li-ion and Na-ion batteries. ACS Appl Energy Mater. 5(1):14 – 19. **https://doi.org/10.1021/acsaem.1c03151**

20. Cui Z, Manthiram A. 2023. Thermal stability and outgassing behaviors of high-nickel cathodes in lithium-ion batteries. Angew Chem Int Ed. 62(43):e202307243. **https://doi.org/10.1002/anie.202307243**

21. Noh HJ, Youn S, Yoon CS, Sun YK. 2013. Comparison of the structural and electrochemical properties of layered Li[NixCoyMnz]O_2 (x = ⅓, 0.5, 0.6, 0.7, 0.8, and 0.85) cathode material for lithium-ion batteries. J Power Sources. 233:121 – 30. **https://doi.org/10.1016/j.jpowsour.2013.01.063**

22. El Moutchou S, Aziam H, Mansori M, Saadoune I. 2022. Thermal stability of lithium-ion batteries: case study of NMC811 and LFP cathode materials. Mater Today: Proc. 51:A1 – A7. **https://doi.org/10.1016/j.matpr.2022.02.324**

Featured Products

Product Description	Cat. No.
Reagents	
Lithium iron phosphate, LFP cathode active material, powder, battery grade	**939420**
Lithium Nickel Manganese Cobalt Oxide NMC532 cathode active material, battery grade	**940968**
Lithium Nickel Manganese Cobalt Oxide NMC811 cathode active material, battery grade	**940925**
Lithium Nickel Manganese Cobalt Oxide, aluminum-doped, NMCA cathode active material	**942960**
Lithium hexafluorophosphate solution in ethylene carbonate, dimethyl carbonate and diethyl carbonate, $LiPF_6$ in EC/DMC/DEC = 1:1:1 (v/v/v) 1.0 m, battery grade	**901685**
Super C65, conductive additive for battery electrode	**940305**
N-Methyl-2-pyrrolidone, anhydrous, 99.5%	**328634**

Related Products

Product Description	Cat. No.
Reagents	
Lithium Nickel Manganese Cobalt Oxide NMC622 cathode active material	**940941**
Lithium Nickel Manganese Cobalt Oxide lithium-niobate coated NMC532 cathode active material	**939579**
Lithium Nickel Manganese Cobalt Oxide lithium-niobate coated NMC622 cathode active material	**939587**
Lithium Nickel Manganese Cobalt Oxide lithium-niobate coated NMC811 cathode active material	**939560**
Super P®, conductive additive for battery electrode	**940259**
Super C45, conductive additive for battery electrode	**940291**
Super C65, conductive additive for battery electrode	**940305**
Carbon nanotube, multi-walled, functionalized powder, L/D ~ 1000, ≥99.9 wt. % MWCNT basis	**928054**
Lithium hexafluorophosphate solution in ethylene carbonate and dimethyl carbonate, 1.0 m $LiPF_6$ in EC/DMC = 50/50 (v/v), battery grade	**746711**

For more information visit us at

Sigmaaldrich.com/battery

MilliporeSigma
400 Summit Drive
Burlington, MA 01803

SigmaAldrich.com

MS_AN14890EN Ver. 1.0 66246 10/2025